Heliyon 10 (2024) e29460

Contents lists available at ScienceDirect

Heliyon

journal homepage: www.cell.com/heliyon

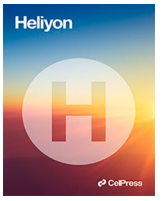

Research article

Structural elucidation and development of azelaic acid loaded mesoporous silica nanoparticles infused gel: Revolutionizing nanodrug delivery for cosmetics and pharmaceuticals

Tahreem Arshad [a], Haji Muhammad Shoaib Khan [a,*], Naveed Akhtar [a], Hanasul Hanan [a], Muhammad Delwar Hussain [b], Mohsin Kazi [c]

[a] Department of Pharmaceutics, Faculty of Pharmacy, The Islamia University of Bahawalpur, Bahawalpur, 63100, Punjab, Pakistan
[b] Department of Pharmaceutical Sciences, School of Pharmacy, University of Maryland Eastern Shore, Princess Anne, MD, 21853, USA
[c] Department of Pharmaceutics, College of Pharmacy, King Saud University, P.O. Box-2457, Riyadh, 11451, Saudi Arabia

ARTICLE INFO

Keywords:
Azelaic acid
Mesoporous silica nanoparticles (MSNs)
Skin permeation study
Tyrosinase inhibition assay
Rheology
Conductivity

ABSTRACT

This research aimed to enhance dermal delivery and optimize depigmentation therapy by designing mesoporous silica nanoparticles (MSNs) encapsulating azelaic acid (AZA) within a gel matrix. The MSNs were prepared using the sol-gel method. After subsequent processes, including acid extraction and drug loading, were then elucidated through PDI, size, zeta-potential, entrapment efficiency, nitrogen adsorption assay, FE-SEM, thermogravimetric analysis, differential scanning calorimetry, Fourier transform infrared spectroscopy, X-ray diffraction, and tyrosinase inhibition assay, were employed to assess the formulation. *In-vitro* stability tests for both AZA-MSN gel (AZCG) and AZA-loaded mesoporous silica gel (AZMG) were conducted at 8 °C, 25 °C, 40 °C, and 40 °C + 75 % RH, encompassing assessments of color, liquefaction, pH, and conductivity. Our findings showed a notable entrapment efficiency of 93.46 % for AZA-MSNs, with FE-SEM illustrating porous spherical MSNs. The particle size of AZA-MSNs was determined to be 211.9 nm, with a pore size of 2.47 nm and XRD analysis confirmed the amorphous state of AZA within the MSN carriers. Rheology examination indicated a non-Newtonian flow, while *ex-vivo* rat skin permeation studies conducted in a phosphate buffer (pH = 5.5) demonstrated a biphasic release pattern with 85.53 % cumulative drug permeation for AZA-MSNs. Overall, the study endorse the potential of AZA-MSNs as an efficacious and stable formulation for AZA delivery, highlighting their promise in addressing pigmentation concerns compared to conventional approaches.

1. Introduction

The skin is the principal organ among other human organs and acts as a shielding layer between the outer environment and humans [1]. Human skin encompasses around 15 % of the total body weight and has a mean surface area of 1.6–2 m^2 [2]. Melanogenesis is a dermatological disorder that causes the skin to become discolored or darker than its natural color (hyperpigmentation). Hormonal

* Corresponding author.
E-mail addresses: tahreemarshad623@gmail.com (T. Arshad), shoaib.khan@iub.edu.pk (H.M. Shoaib Khan), nakhtar567@gmail.com (N. Akhtar), hanasulhanan1012@gmail.com (H. Hanan), delwarcc@gmail.com (M.D. Hussain), mkazi@ksu.edu.sa (M. Kazi).

https://doi.org/10.1016/j.heliyon.2024.e29460
Received 2 February 2024; Received in revised form 7 April 2024; Accepted 8 April 2024
Available online 13 April 2024

List of abbreviations

Abbreviations	*Full forms*
AZA	Azelaic Acid
MSNs	Mesoporous Silica Nanoparticles
AZA-MSN	Azelaic Acid Loaded Mesoporous Silica Nanoparticles
AZCG	Azelaic Acid Control Gel
AZMG	Azelaic Acid MSNs Gel
EE%	Entrapment Efficiency
TGA	Thermogravimetric Analysis
ANOVA	Analysis Of Variance
LSD	Least Significant Difference
RH	Relative Humidity
DSC	Triethanolamine
BET	Brunauer-Emmett-Teller
TEOS	Tetraethyl Orthosilicate
CTAB	Cetyltrimethylammonium Bromide
XRD	X-Ray Diffraction
FTIR	Fourier Transform Infrared Spectroscopy
FE-SEM	Field Emission Scanning Electron Microscopy

changes, wounds, inflammation, acne, dermatitis, some medications, and UV radiation can all cause changes in skin tone [3]. Melanin, a skin pigment, and melanocytes, which are melanin-producing cells found in various skin layers, control the process of skin pigmentation and coloration [4]. Although hyperpigmentation is not lethal, it can lower patients' standard of life by impairing their mental and emotional health. Tyrosinase inhibition is the most widely used approach for treating hyperpigmentation because it is the most important enzyme in the melanogenesis process [5]. Compared to other conventional therapies for hyperpigmentation, conventional topical therapies have several drawbacks because of their poor stability and decreased permeability [6]. The need for innovative therapeutic approaches is unmet since there is currently no proven treatment that can completely cure hyperpigmentation.

Mesoporous silica nanoparticles are among the inorganic nanomaterials that have a special adsorption capability, low density, and good biocompatibility, making them a striking contender for a range of biomedical therapies [7]. MSNs are among the silica materials that have a variety of exceptional and useful structural characteristics, including modular morphology (size and shape), huge surface area (>700 m^2/g), tunable pore diameter (2–10 nm), larger pore volume (>1 cm^3/g), and three distinct practical areas (the outer particle surface, silica framework, and inner pore surface). Excessive drug loading is primarily facilitated by the huge area and pore volume of these materials [7,8].

Azelaic acid is a dicarboxylic acid that occurs naturally and has been exploited extensively to cure hyperpigmentation diseases and pimples [9]. Azelaic acid has excellent tolerance, has no side effects, and is similar to 4 % hydroquinone and superior to 2 % hydroquinone in extensive clinical trials of hyperpigmentation disorders [10]. Azelaic acid has great safety and tolerability qualities [11]. AZA, also identified as 1,7-heptane dicarboxylic acid, has been shown to have skin-rejuvenating effects on certain hyperpigmentation disorders. It is an *in-vitro* inhibitor of tyrosinase [12]. There are no harmful systemic effects or mutagenic, phototoxic, or teratogenic consequences of azelaic acid [13,14]. For the treatment of hyperpigmentation, doses ranging from 15 % to 20 % are utilized [15]. Additionally, it reduces the generation of free radicals, which may help to improve skin renewal [16]. However, to obtain the intended therapeutic effect, an additional dose of AZA is frequently needed because of its low solubility and lack of skin penetrability [17]. MSNs are inorganic silica materials with a variety of remarkable and useful structural characteristics. Moreover, important molecules can be carried by silica nanoparticles, which enhance their stability, permeability, and resistance to degradation [7,18]. Silica is more prevalent than other nanoparticles (NPs) and has developed biocompatibility scores. MSNs are more resistant to exterior responses such as mechanical stress and degradation than other materials [19,20].

This research is a novel approach to dermal nanodrug delivery technology, particularly in the field of dermatology, where MSNs have seen limited exploration. By exploiting the unique features of MSNs and combining them into a gel matrix, we are redefining nanodrug delivery, enabling increased efficacy, and enhanced penetration of azelaic acid for cosmetic and dermatological purposes. This novel composition shows promise for addressing numerous skin diseases successfully while reducing undesirable effects, hence paving the door for compelling breakthroughs in skincare and dermatological therapies. As previously discussed, mesoporous silica nanoparticles have a huge pore volume, good porosity, large surface area, and high drug loading. All these abovementioned factors are critical for designing azelaic acid-encapsulated MSN-infused gels for advanced topical skin rejuvenation and depigmentation therapy. In the present study, we aimed to synthesize azelaic acid-encapsulated MSN-infused gels. The fabricated mesoporous silica nanoparticles were structurally elucidated by using particle size analysis, PDI, zeta potential, FESEM, entrapment efficiency, XRD, DSC, TGA, FTIR, pore size, surface area, pore volume, and N_2 adsorption-desorption assays and *in-vitro* evaluation were also performed for the stability assessment of AZA-MSNs-infused gel.

2. Methodology

2.1. Materials

Azelaic acid, ethanol, sodium hydroxide, mushroom tyrosinase, and cetyl trimethyl ammonium bromide (CTAB) were acquired from Sigma Aldrich (Taufkirchen, Germany). Tetraethyl orthosilicate (TEOS) was acquired from Merck (Darmstadt, Germany), and Carbopol 940 was taken from VWR (Radnor, PA, USA). and triethanolamine was bought from Daejung, Korea. Deionized water was obtained from the Department of Pharmaceutics, The Islamia University of Bahawalpur. All the other chemicals used were of analytical grade.

2.2. Synthesis of MSNs

The preparation of MSNs was carried out according to the sol-gel method utilizing CTAB as a surface-active agent or template [21]. First, 1g of CTAB is carefully weighed and dissolved in 450 ml of deionized water with a stirrer set to 500 rpm at 25 °C. After adding 3.5 ml of 2 M NaOH solution, raise the temperature to 80 °C and stir at 600 rpm to achieve a clear solution. Maintaining the temperature at 80 °C for 30 min, 5 ml of TEOS is slowly added at a rate of 0.33 ml/min while stirring at 800 rpm for 2 h. A suspension with white precipitates is formed as a result of this process. The MSNs are then collected by centrifugation at 14,000 rpm for 15–20 min at room temperature. The gathered MSNs are washed with methanol and water to remove any unreacted material and then dried for 24 h. Acid extraction was carried out to remove the surfactant in 100 mL of methanol, 1.0 mL of concentrated hydrochloric acid, and 1.0 g of MSNs containing the surfactant at 60 °C. The template-free MSNs were gathered by centrifugation at the speed of 14000 rpm for 15 min, cleaned with water and methanol, and dried for 24 h at 60 °C [22].

2.3. Loading of azelaic acid into MSNs

To initiate the process, a solution of azelaic acid was made by dispersing 1 mg/mL in 10 mL of methanol. Following this, 10 mg of MSNs were added to the azelaic acid solution. The resulting blend was stirred at 100 revolutions per minute in a dark atmosphere for 24 h, with a temperature of 25 °C. Following the specified incubation period, azelaic acid-loaded MSNs were separated to remove any unbound azelaic acid. This separation was obtained by centrifugation at 16,000 rpm for 30 min then azelaic acid-loaded MSNs were rinsed three times with deionized water, dried, and appropriately kept for future use [23] (Fig. 1).

2.4. Formulation of the AZA-MSN infused gel (AZMG)

Gels were prepared with 2 % Carbopol 940 using a homogenizer (Euro-Star, IKA D 230, Germany) at the speed of 1500 rpm for 20 min and the pH was adjusted by using triethanolamine. After gel preparation, 15 % azelaic acid-loaded MSNs were gradually incorporated into the gel during homogenization. Homogenization resumed until a consistent gel was established. The pH of the gel was corrected from 6 to 6.5. The whole method to formulate AZA-MSN infused gel is depicted in Fig. 1.

Fig. 1. Synthesis of AZA-MSNs-infused gel.

2.5. Formulation of the control gel containing azelaic acid (AZCG)

During homogenization, 2 % of the Carbopol 940 and 15 % of the azelaic acid were added to distilled water to prepare the simple gel. We used triethanolamine to decrease the pH. Until a homogeneous gel was achieved, homogenization was maintained.

2.6. In-vitro studies

2.6.1. Characterization of MSNs

2.6.1.1. PDI, zeta potential, and particle size. The PDI, particle size, and zeta potential of the MSNs and AZA-MSNs were determined in triplicate by utilizing a Malvern Zetasizer. MSN suspensions with concentrations of 100 mg/L were prepared using deionized water as a dispersant. The measurements were recorded at 25 °C.

2.6.1.2. Field emission scanning electron microscopy (FE-SEM). Field emission scanning electron microscopy (FE-SEM) was used to inspect the surface morphology and shape of the mesoporous silica nanoparticles (MSNs). Before imaging, the samples were decorated with gold. FE-SEM images were captured at various amplifications.

2.6.1.3. Entrapment efficiency (EE%). EE was evaluated indirectly by finding out the amount of unentrapped drugs. After mixing 10 mg of azelaic acid in 10 mL of methanol, 10 mg of mesoporous silica nanoparticles (MSNs) were poured into the azelaic acid solution. The blend was stirred in the darkness for 24 h at 25 °C. The azelaic acid-loaded MSNs were collected by centrifugation at 16000 rpm for 30 min until a supernatant was formed to separate the free azelaic acid. After the supernatant was extracted from the sediments, the absorbance was measured using a spectrophotometer for analysis. The formula to calculate the EE% is given below [24].

$$\%\boldsymbol{Entrapment\ Efficiency} = (\boldsymbol{T} - \boldsymbol{F}) \div \boldsymbol{T} \times \mathbf{100}$$

Where T is the total amount of initial drug f and F is the amount of unloaded drug in the supernatant.

2.6.1.4. Nitrogen adsorption assay. The nitrogen adsorption experiment was carried out under N2 utilizing BET (ASAP2020, USA) with a degassing temperature of 150 °C and a degassing period of 6 h. From the nitrogen desorption isotherms, BET techniques were utilized to calculate the average particle area, average volume, and average pore size of the MSNs and AZMSNs [25].

2.6.1.5. Thermal analysis. TGA and DSC were used to assess the thermal characteristics and thermal composition of AZA, AZA-MSNs, and MSNs. Using a Simultaneous Thermal Analyzer (STA) STA 6000/8000-PerkinElmer, 5–10 mg of AZA, AZA-MSN, and MSN were heated at a rate of 10 °C/min from 31 to 500 °C in a TGA alumina crucible underneath a nitrogen purge of 20.0 ml/min [26].

2.6.1.6. Fourier transform infrared spectroscopy (FTIR). FTIR spectroscopy was used to investigate the functional groups and interactions between various components of the MSNs by using Tensor 27 FTIR (Bruker Optics GmbH; Ettlingen, Germany). FTIR spectra were acquired over the spectral range using the KBr pellet method. FTIR analyses of azelaic acid, MSNs, and azelaic acid-loaded MSNs (AZMSNs) were performed [27].

2.6.1.7. XRD. An X-ray diffractiometer (Philips X'pert, Netherlands) fitted with a liquid nitrogen-cooled germanium solid-state detector and Cu Kα radiation was used to obtain the XRD patterns of the AZA, AZA-MSN, and MSN samples. Thirty mA and thirty kV were used to produce the X-rays. The data were collected at a step size of 0.020° and an inspecting velocity of 4°/min radiation from 5° to 80° (diffraction angle 2θ) [28].

2.6.2. Anti-tyrosinase assay

Mushroom tyrosinase was used as the enzyme source in an *in-vitro* tyrosinase assay. The inhibitor was selected at concentrations of 10, 20, 30, and 40 mM/ml. Tyrosinase enzyme (5600 units/ml) and phosphate buffer solution (50 mM) were added to the reaction mix, which was then incubated for 10 min at room temperature. After incubation, 10 mM L-DOPA was incorporated as a substrate. The ingredients were mixed and then incubated for an additional half hour. Kojic acid was employed as the (+) control. Every sample was assessed 3 times. A Labtech LT-4500 was used to take the absorbance of the microplate wells at 475 nm. The percent tyrosinase inhibition was calculated with the help of the formula below [29].

$$\text{Inhibition}(\%) = \frac{\textbf{Absorbance of test solution}}{\textbf{Absorbance of control}} \times \mathbf{100}$$

2.6.3. Ex vivo permeation study

In-vitro drug permeation examinations were conducted in a 1.76 cm2 Franz diffusion cell for 12 h. The diffusion membrane was made from recently excised albino rat skin. The skin was submerged in pH 5.5 phosphate buffer overnight to activate the fungus. Phosphate buffer (pH 5.5) was used as the receptor medium. Rat skin was placed between the donor and receptor compartments, with the stratum corneum facing the donor compartment. The warmth of the cell was retained at 37 °C. The skin of the donor compartment

was covered with 1 g of sample (AZCG and AZMG gel). For the samples to penetrate through the skin and enter, the receptor media and the skin must be linked. For the samples to penetrate through the skin and enter the medium, the skin and the receptor media must be linked. One milliliter aliquot was removed from the recipient medium at prearranged intervals of 30 min, 1 h, 2 h, 3 h, 4 h, 5 h, 6 h, 7 h, 8 h, and 12 h to maintain sink conditions. A new phosphate buffer was then added to these aliquots. The amount of medication that had penetrated the skin was measured with a UV spectrophotometer. Several penetration criteria can be determined by charting the cumulative amount of medication taken over time [30].

2.6.4. Stability study of the AZMG and AZCG formulations

For three months, stability tests were conducted on control MSN gels containing azelaic acid at four various temperatures (8 °C, 25 °C, 40 °C, and 40 °C ± 75 % RH). The organoleptic, pH, and rheological properties of the samples were estimated at predetermined intervals.

2.6.4.1. Organoleptic estimation. The organoleptic characteristics (color and liquefaction) of the AZCG and AZMG formulations stored at four different temperatures were determined for 3 months at specific time intervals.

2.6.4.2. Rheology. The Rheology of AZCG and AZMG was performed at various temperatures at specific time intervals for 3 months by utilizing a DV-III Ultra Rheometer (Brookfield Engineering Laboratories, Inc.). Samples (AZMG and AZCG) weighing 0.5 g were placed on a rheometer plate for analysis. Values were obtained by continuously increasing the shear rate between 10 and 100 rpm. Beforehand any readings were taken, the shear rate was held constant for 10 s to examine the rheological changes. The program Rheocalc V-2.6 was employed to analyze the data [31].

2.6.4.3. pH variation. Using a pH meter, the pH of AZCG and AZMG was acquired. To determine the pH on the screen, the pH meter electrodes were dipped into the samples. Three duplicate readings were taken, and the average was calculated. A statistical scrutiny of the pH fluctuations was made, and a graphical record of the pH against time was produced.

2.6.4.4. Conductivity measurements. A conductivity meter was employed to measure the conductivity of the AZCG and AZMG formulations. Measurements were directed in triplicate, and the average value was calculated. Statistical analysis was employed to examine the conductivity variations over the 3-month duration, and a graphical representation of conductivity versus time was generated.

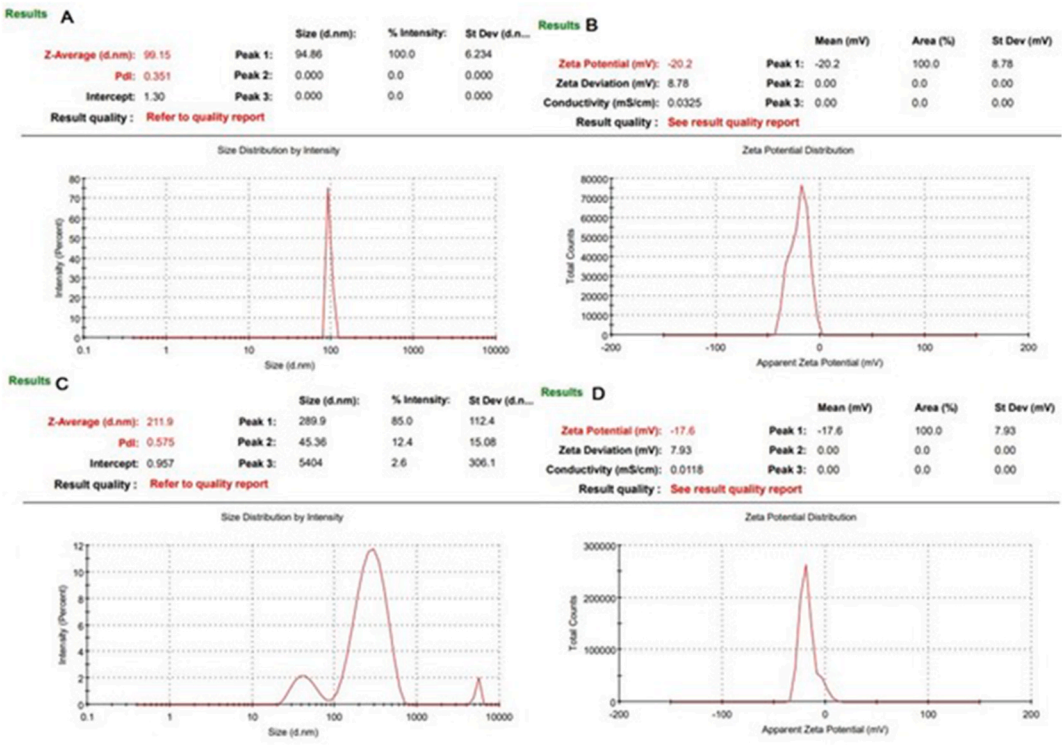

Fig. 2. PDI, zeta potential, and particle size of unloaded (A, B) and loaded (C, D) MSNs.

2.7. Statistical analysis

Acquired data was evaluated statistically by using SPSS version 20. For data comparison and multiple comparisons of control and MSN gels of azelaic acid, two-way ANOVA with LSD and paired sample *t*-test were used, respectively. $P < 0.05$ was chosen as the threshold for statistical significance. The use of two-way ANOVA allowed us to investigate the effects of both temperature and time simultaneously on the formulations. Additionally, we conducted a paired sample *t*-test to further evaluate the performance of all AZCG and AZMG formulations under different storage conditions. This statistical test enabled us to compare the means of paired samples (e.g., AZCG and AZMG formulations) to determine whether there were significant differences in their performance across various storage conditions. Statistical analyses were employed on pH, rheology, and conductivity findings.

3. Results and discussion

3.1. In-vitro studies

3.1.1. Characterization of MSNs

3.1.1.1. PDI, zeta potential, and particle size. As previously stated, a Zetasizer was used to determine the particle size. As illustrated in Fig. 2 (A, C), the particle size of the drug-free MSNs was measured to be 99.15 nm, whereas the particle size of the mesoporous silica nanoparticles loaded with azelaic acid was measured to be 211.9 nm. Fig. 2 (A, C) displays the polydispersity indices (PDIs) for MSNs and AZA-MSNs, which are 0.351 and 0.575, respectively. PDI contributes to high homogeneity and results in a narrow size distribution of MSNs. The zeta potential is used to quantify electrostatic repulsion or particle size. The electrostatic repulsive forces in a system should outweigh the attractive van der Waals forces for the system to be stable, according to the DLVO theory [32]. This is because the physical constancy of any dispersed system increases with increasing electrostatic repulsion energy, which is proportional to the width of the diffusing sheet and charge. The zeta potential is a crucial measure of MSN stability. The stability of MSNs increases with increasing zeta potential [33]. MSNs are (−) charged because of silanol group occurrence, which prevents aggregation and increases their stability. Fig. 2 (B, D) displays the zeta potential values of MSNs and AZA-MSNs, which are −20.2 and −17.6, respectively.

Furthermore, the negative zeta potential values in MSNs and AZA-MSNs show electrostatic repulsion, which contributes to the stability of the nanoparticle formulations [34]. These promising findings show that AZA-MSNs have the potential to be useful carriers for anti-pigmentation therapy, providing increased stability and better treatment effects.

3.1.1.2. Field emission scanning electron microscopy (FE-SEM). Using FE-SEM, the morphology and porous structure of the MSNs were examined. The virtually monodispersed spherical shape of the MSNs was revealed using FE-SEM micrographs. Furthermore, FE-SEM unequivocally demonstrated the presence of mesostructures and confirmed the existence of pores. The MSN sample SEM images at 100,000× and 200,000× magnifications are displayed in Fig. 3A and B, respectively.

3.1.1.3. Entrapment efficiency (EE%). With the usage of a UV–visible spectrophotometer and PBS buffer (pH = 5.5) at 240 nm, the effectiveness of azelaic acid entrapment inside mesoporous silica nanoparticles (MSNs) was measured, and the value was 93.46 % by employing an indirect method and successful incorporation of AZA in MSNs was further confirmed by the FTIR and XRD analysis as displayed in Fig. 5. It has been suggested that obtaining a high drug-loading content is beneficial because of the silanol groups on MSNs surface, which offer active sites for attachment to drug molecules [35,36]. We explained this phenomenon by saying silanol groups and AZA molecules formed hydrogen bonds. Overall, the high entrapment efficiency contributes to the stability of the nanoparticles and enhances their biological performance by ensuring a sufficient amount of drug is delivered to the target site, thereby improving the efficacy of anti-pigmentation therapy [37].

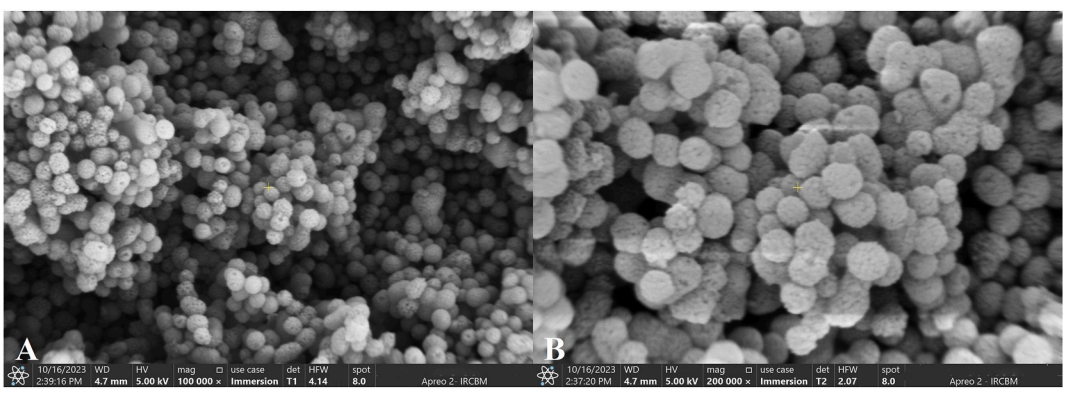

Fig. 3. FE-SEM images of mesoporous silica nanoparticles at 100,000× (A) and 200,000× (B) magnifications.

3.1.1.4. Nitrogen adsorption assay. According to the IUPAC classification, the N2 adsorption/desorption isotherm of MSNs, as illustrated in Fig. 4A, possibly categorized as a type IV isotherm with a hysteresis loop [38] while, the N2 adsorption/desorption isotherm of AZA-MSNs, as illustrated in Fig. 4B. It is possible to explain the noticed hysteresis loop at elevated relative pressure (approximately 0.8) to the inter-particle porosity, a characteristic that is frequently reported for silica mesoporous materials that are manufactured similarly [39,40]. The surface area, pore volume, and pore size of the MSNs and AZA-MSNs are displayed in Table 1. Based on the results from the adsorption branch, the pore diameter was calculated. As a result, all these results point to the well-ordered mesoporous structure of the MSNs employed in this study. The pore size, pore volume, and surface area data are listed in Table 1 to further verify the successful integration of AZA into the MSNs. Compared to those of MSNs, the pore size, pore volume, and surface area of AZA-MSNs were much smaller. The effective loading of AZA-MSNs into the pores of MSNs was validated by these findings [41]. Furthermore, the smaller pore size found in AZA-loaded MSNs may improve cellular uptake efficiency, increasing drug bioavailability and treatment efficacy. Furthermore, the isotherm's structural integrity promotes physical stability by keeping the nanoparticles' size, shape, and surface properties constant during storage and administration [42]. Furthermore, the stable mesoporous silica structure protects encapsulated pharmaceuticals such as azelaic acid (AZA) against chemical degradation while maintaining their efficacy over time [43]. In conclusion, the N2 adsorption/desorption isotherm is an important tool for understanding the structural features of MSNs, which have a direct impact on their performance and stability in anti-pigmentation therapy, ultimately adding to their success in treating pigmentation issues.

3.1.1.5. Thermal analysis. Using TGA (mass versus temperature), the drug entrapping efficiency and thermal constancy of MSNs, AZA-MSNs, and AZA were assessed. The evaporation of ingested water molecules is responsible for 16.88 % of the loss that MSNs experienced between 10 and 500 °C, as shown by the results in Fig. 3C. These results proved that MSNs are hydrophilic, which makes them appropriate for encapsulating medications with poor water solubility [44,45]. AZA demonstrated a one-step thermal breakdown at 200–300 °C, which accounted for 91.71 % of the mass loss. AZA-MSN exhibited a large loss of 23.32 % from 91.71 %. This means that there was a 68.39 % difference in mass loss between AZA-MSN and AZA, which can be explained by the fact that AZA was added to the MSNs and protected from degradation (Fig. 4C). Furthermore, AZA-MSNs demonstrate enhanced thermal stability compared to free

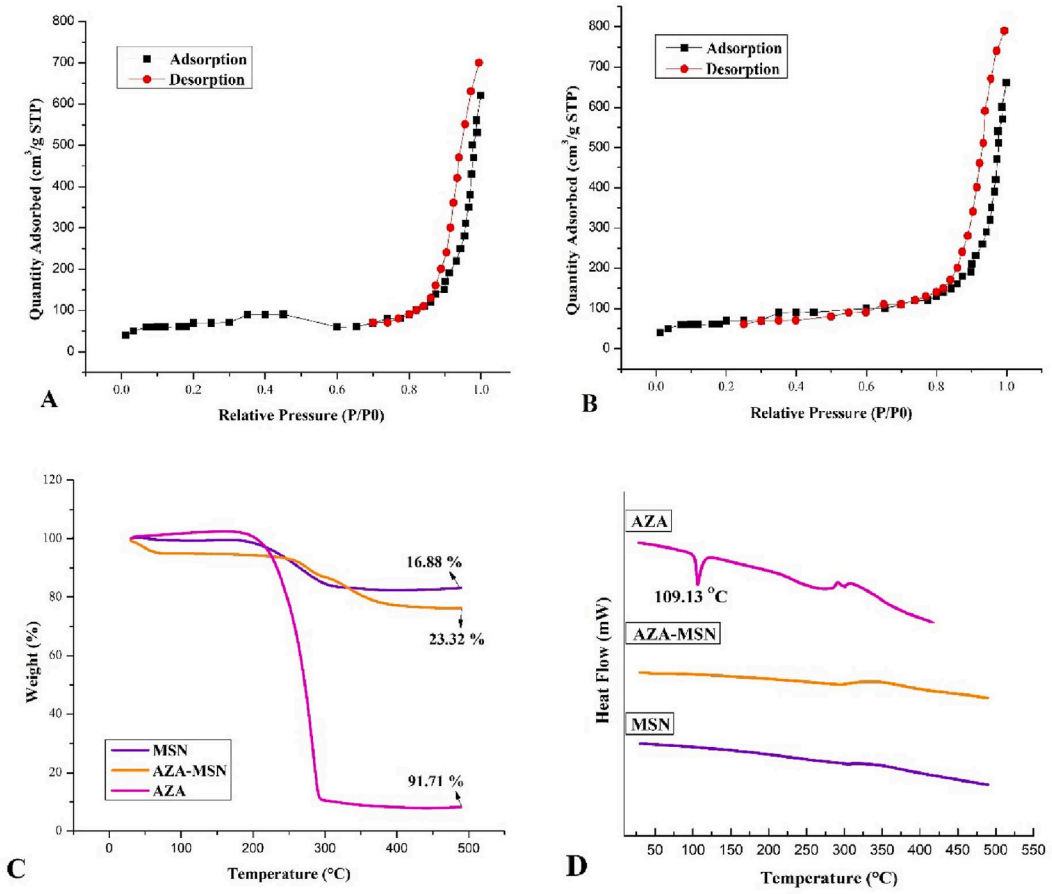

Fig. 4. Adsorption/desorption isotherms of MSNs (A) and AZA-MSNs (B), (C) TGA thermograms, and (D) differential scanning calorimetry thermograms of AZA, AZA-MSNs, and MSNs.

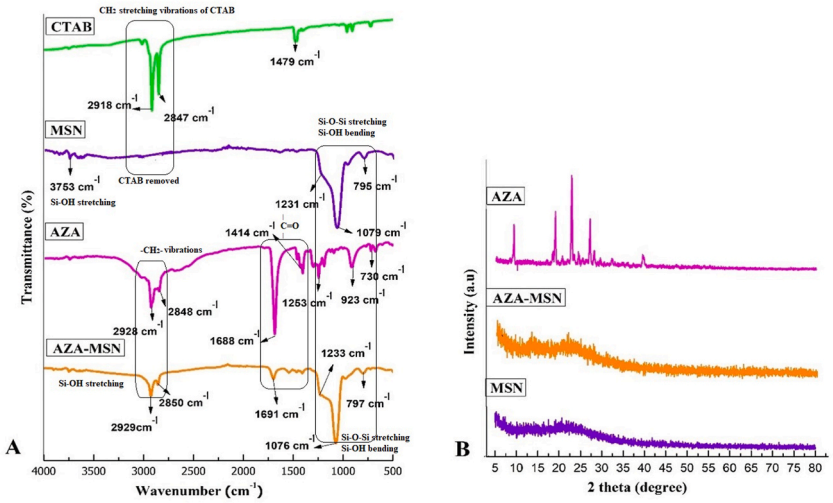

Fig. 5. (A) FTIR spectra of CTAB, MSNs, AZA and AZA-MSNs. (B) XRD patterns of AZA, MSNs, and AZA-MSNs.

Table 1
Porosity characteristics of MSNs before and after loading with AZA.

Samples	Surface area (m^2/g)	Pore volume (cm^3/g)	Pore size (nm)
MSN	752.22	0.64	3.45
AZA-MSN	602.50	0.38	2.47

AZA, suggesting protection against degradation when encapsulated within MSNs. This improved stability ensures the preservation of the drug's potency during storage and administration, ultimately enhancing its efficacy in addressing pigmentation concerns [21,46]. The occurrence or absence of AZA in the MSN pores was confirmed by DSC analysis. According to Fig. 4D–AZA exhibited a melting endothermic peak at 109.13 °C, confirming the crystalline form of the drug and supporting previous research [47]. The drug loading into MSNs was confirmed by the absence of an endothermic peak corresponding to azelaic acid in the drug-laden particles, revealing that the drug was successfully entrapped into the particles and was in an amorphous state. Additionally, DSC analysis confirms the successful encapsulation of AZA within MSNs, further supporting the formulation's stability and performance. In conclusion, thermal analysis provides valuable insights into the stability and drug loading capabilities of MSNs, which are essential for optimizing their biological performance and stability in anti-pigmentation therapy [21].

3.1.1.6. Fourier transform infrared spectroscopy (FTIR). Because cetyltrimethylammonium bromide (CTAB) is known to be harmful, FTIR testing was executed to ensure that the template was removed from the nanoparticles. The C–H stretching of the methylene groups in CTAB (near the quaternary ammonium cation) is represented by two peaks in the IR spectra (Fig. 5A) at 2918 cm^{-1} and 2847 cm^{-1}. The effective extraction of CTAB from the nanoparticles was demonstrated by the disappearance of these peaks in the MSN spectrum. The absorption band at 3753 cm^{-1} for spectrum MSNs is caused by the vibrational frequency of the stretching of the surface hydroxyl groups of silanol. Fig. 5A displays the FTIR spectra of the MSNs, which include a prominent band at 1079 cm^{-1} and two less prominent bands at 795 cm^{-1} that represent the vibration absorption of Si–O–Si groups [48]. Additionally, the effective loading of AZA into MSNs and the extraction of CTAB from MSNs were verified by FTIR spectroscopy (Fig. 5A). Significant absorption peaks were observed in the FTIR spectrum of AZA at 730, 923, 1253, 1414, 1688, 2848, and 2928 cm^{-1}. Hsieh et al. identified similar FTIR peaks for azelaic acid [49].The bandwidth at approximately 1076 cm^{-1} and the Si–*O*–Si groups characterize the AZA-loaded MSN spectrum. The stretching of the AZA drug-loaded MSNs is represented by the peaks at 1691 cm^{-1}, 2929 cm^{-1}, and 2850 cm^{-1}. The successful encapsulation of the chosen model drug into the MSNs was further confirmed by the appearance of these broad peaks. Where the oxygen atom plays the role of a bridge between two silicon sites**.** FTIR is important in evaluating the biological performance and stability of mesoporous silica nanoparticles (MSNs) because it confirms the removal of harmful compounds like cetyltrimethylammonium bromide and the effective loading of drugs like azelaic acid (AZA) [46]. This encapsulation improves the stability of AZA, preserving it from degradation and contributing to the nanoparticles' overall effectiveness in anti-pigmentation therapy. Overall, FTIR spectroscopy gives useful information about MSN composition and structure, allowing for the evaluation of their biological efficacy and stability in therapeutic applications.

3.1.1.7. XRD. Fig. 5B shows the results of the XRD studies of AZA, AZA-MSN, and MSN. The detection of crystallinity of AZA was accomplished by XRD analysis, which was also anticipated to yield oblique proof of AZA's successful entrapment within MSNs. Five unique characteristic peaks of AZA were observed to be located at 9.22°, 18.96°, 22.72°, 27.02°, and 39.50° [50]. However, because

MSNs are amorphous, they did not exhibit any discernible diffraction peaks indicating that MSNs were single-phase material, as seen in Fig. 5B. The XRD pattern of AZA-MSN (Fig. 5B) did not show any crystalline AZA following incorporation into MSN, indicating that the AZA was incorporated into MSNs carriers in an amorphous condition [45,51]. It was assumed that space confinement, which left the AZA in a disordered amorphous condition, inhibited the AZA from crystallizing when it was loaded into the small pores and mesoscopic channels of MSNs [52]. Importantly, the amorphous state of AZA within MSNs increases its stability, avoiding crystallization-induced degradation, thus contributing to the overall effectiveness of the nanoparticles in anti-pigmentation therapy [46].

3.1.2. Anti-tyrosinase assay

Tyrosinase, an enzyme that is essential for the synthesis of melanin, can be inhibited to stop the production of melanin pigment, which can help treat skin conditions that cause excessive pigmentation. A literature review further confirmed that a special enzyme source for researching the *in-vitro* anti-tyrosinase action of depigmentation treatments is mushroom tyrosinase [53,54]. To produce melanin, tyrosinase is an essential enzyme that is found in both humans and animals. For this reason, it is considered a key enzyme in the study of human melanogenic processes. Fig. 6 shows that, compared with AZA-MSNs, AZA has a very good tyrosinase inhibitory effect, suggesting that azelaic acid was successfully loaded into the MSNs. Azelaic acid, also called 1,7-heptane dicarboxylic acid, is effective at curing certain hyperpigmentation conditions due to its competitive inhibitory effect on tyrosinase *in-vitro* [12]. This result highlights the promise of AZA-MSNs as a delivery vehicle for azelaic acid, demonstrating their capacity to maintain the drug's effectiveness while increasing its stability [53,54]. Overall, the anti-tyrosinase assay is an important technique for assessing nanoparticles' biological performance in reducing melanin synthesis and treating hyperpigmentation, providing useful information about their efficacy and prospective clinical uses.

3.1.3. Ex vivo permeation study

To evaluate the penetrating property of the MSN gel loaded with azelaic acid in comparison to that of the control gel containing azelaic acid from the stratum corneum, permeation research was conducted. AZMG and AZCG had steady-state fluxes of 87.03 and 39.05 μg/cm^2/h, respectively. The enormous pore capacity, nanosized nature, and exceptionally large surface area of mesoporous silica nanoparticles all contribute to their enhanced ability to permeate biological skin membranes and boost medication penetration. Numerous investigations have documented how skin penetration amplifies the function of mesoporous silica nanoparticles for various drug loads [55,56]. Fig. 7D shows the cumulative azelaic acid permeation percentage over time. For AZMG, the cumulative drug concentration was 85.53 %, which was significantly greater than that of AZCG (43.15 %) (Fig. 7D). The *ex vivo* permeation investigation provides insight into the biological performance and stability of mesoporous silica nanoparticles (MSNs) loaded with azelaic acid, specifically their capacity to enter epidermal membranes and improve drug delivery.

3.1.4. Stability study of AZMG and AZCG formulations

3.1.4.1. Organoleptic evaluation. Organoleptic characterization was performed on materials stored at four different temperatures, including color and liquefaction analysis. Interestingly, no color changes were observed for up to three months at 8 °C or 25 °C for AZCG or AZMG. Nevertheless, after three months at an elevated temperature of 40 °C, the AZCG lost its stability. On the 28th day, at 40 °C + 75 % RH, the color of the AZCG began to change, indicating gel instability. Similarly, AZMG became whitish to somewhat yellow in the third month and became unstable at elevated temperatures of 40 °C and 40 °C + 75 % RH. Table 2 presents the information.

Centrifugation was used to verify the physical constancy of the formulation. The foundation of this process is the phase separation caused by variations in density under centrifugal shear [31]. Interestingly, AZMG showed no signs of liquefaction at any temperature.

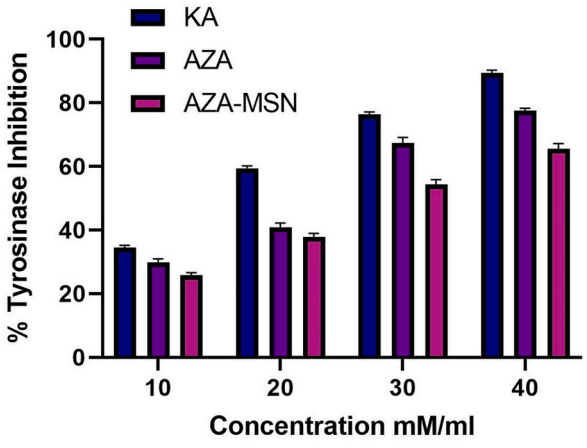

Fig. 6. Anti-tyrosinase activity of KA (kojic acid), AZA, and AZA-MSNs.

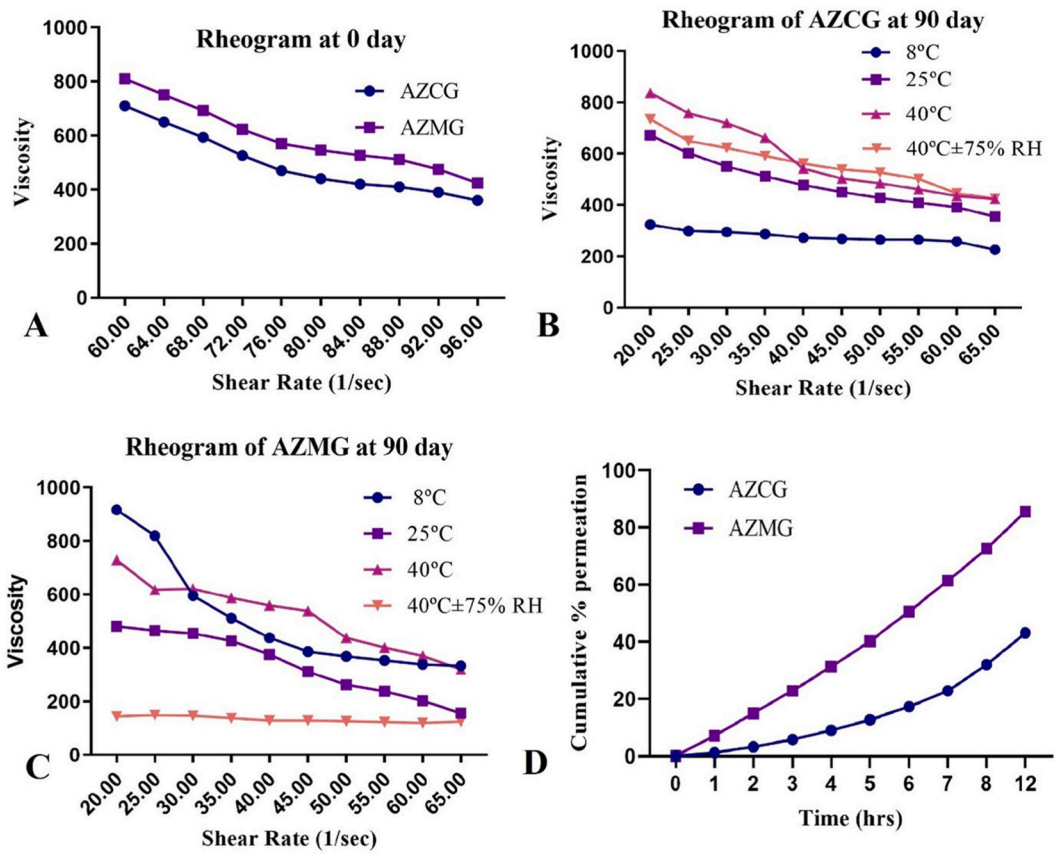

Fig. 7. Rheology at 0 day (A) versus at 90 day of AZCG (B) and AZMG (C). *Ex vivo* skin permeation profiles (D).

Table 2
Organoleptic properties of AZCG and AZMG under various storage conditions.

Organoleptic parameters	Formulation	Temperature	Time (Days)					
			Zero	7th	14th	28th	60	90
Color	AZCG	8 °C	W	W	W	W	W	W
		25 °C	W	W	W	W	W	W
		40 °C	W	W	W	W	W	SY
		40 °C ± 75%RH	W	W	W	SY	SY	Y
	AZMG	8 °C	W	W	W	W	W	W
		25 °C	W	W	W	W	W	W
		40 °C	W	W	W	W	W	SY
		40 °C ± 75%RH	W	W	W	W	SY	SY
Liquefaction	AZCG	8 °C	–	–	–	–	–	–
		25 °C	–	–	–	–	–	–
		40 °C	–	–	–	–	+	+
		40 °C ± 75%RH	–	–	–	–	+	+
	AZMG	8 °C	–	–	–	–	–	–
		25 °C	–	–	–	–	–	–
		40 °C	–	–	–	–	–	–
		40 °C ± 75%RH	–	–	-	–	–	–

W = white, SY = slight yellow, -ve = negative, +ve = positive, AZCG = azelaic acid control gel, AZMG = azelaic acid MSN gel.

Similarly, throughout the trial, AZCG also held steady at lesser temperatures (8 °C and 25 °C) (Table 2).

3.1.4.2. Rheological study. Rheological characterization is a useful procedure for assessing the effectiveness and caliber of cosmetic products [57]. It is also crucial for predicting bodily stability [58]. All the rheograms showed that viscosity decreases with increasing shear rate. The shear stress and viscosity are inversely correlated with the shear rate, as illustrated in Fig. 7 (A, B, C). This inverse relationship results from the formulation's generation of aggregates in the absence of shear stress. These clumps disintegrate under

stress, which lowers the viscosity. Based on the different temperatures and time intervals, two-way ANOVA exposed a significant ($p < 0.05$) change in viscosity for both the AZCG and AZMG formulations. The viscosity of the AZCG and AZMG formulations was significantly ($p < 0.05$) correlated according to paired sample t-tests.

However, with AZMG maintained at 8 °C 25 °C 40 °C and 40 °C + 75 % RH, the decrease in viscosity was negligible ($P \geq 0.05$). According to the previously mentioned observations, viscosity changes because of applied shear stress, indicate the pseudoplastic non-Newtonian behavior of gels [59]. In other words, thinning qualities are observed in gels when shear stress is applied, and shear strain is created. This attribute implies that the formulations display thinning properties under applied shear stress, allowing for easier application and spreadability on the skin [31]. Rheological characterization provides useful insights into the biological performance and stability of MSN-containing cosmetic formulations, allowing for the development of effective and stable topical treatments.

3.1.4.3. pH variation. For three months, the MSN and control gels were stored at various temperatures, and their pH was routinely checked. The pH of the dermal layer ranges from 4.1 to 5.8, making it mildly acidic [30]. The freshly synthesized AZCG and AZMG in this study had pH values of 6.6 and 6.8, respectively. The pH of the AZCG and AZMG formulations decreased from the first day to 90 days, as shown in Fig. 8A and B, respectively. A two-way analysis of variance was used to validate the difference in pH between the AZCG and AZMG formulations. The results showed that the pH fluctuation was statistically significant ($p < 0.05$) concerning temperature and time. A paired sample *t*-test was used to evaluate the performance of all the AZCG and AZMG formulations under different storage conditions. The pH levels of AZCG and AZMG differed significantly. pH stability ensures optimal skin compatibility and therapeutic efficacy of the MSN gels containing AZA, favoring their effectiveness in treating skin concerns [30,60].

3.1.4.4. Conductivity measurements. Electrical conductivity is a measurement of free ions [61]. The electrical conductivity of the AZCG and AZMG gels was measured during three months at various storage temperatures (8 °C, 25 °C, 40 °C, and 40 °C with 75 % RH) as shown in Fig. 9A and B, respectively. The results show a small rise in conductivity from freshly made gels to the 3-month mark, indicating subtle changes in electrical characteristics. Several variables may account for the small increase in conductivity [62,63]. First, it could be influenced by the gel matrix's aging process as well as interactions between components, including MSNs. Furthermore, environmental factors such as temperature and humidity could have influenced the electrical characteristics of the formulations during the three-month storage period. Finally, the observed trends in conductivity alterations from initial preparation to 3-month storage provide important insights into the stability and behavior of AZCG and AZMG formulations. Fig. 9 shows the trend of electrical conductivity. First, conductivity affects nanoparticle penetration through biological barriers such as the skin, potentially enabling therapeutic drug distribution to target areas. Changes in conductivity may also have an impact on drug release from nanoparticles, resulting in better drug control and more successful therapeutic effects. Furthermore, variations in conductivity can indicate changes in the stability of nanoparticle formulations, limiting aggregation or degradation over time while preserving medication effectiveness. Finally, maintaining optimal conductivity levels enables compatibility with biological systems, hence improving biological performance and medicinal efficacy [30,64].

4. Conclusion

This research presents a significant novelty in cutaneous nanodrug delivery technology, particularly in the field of dermatology, where MSNs have seen limited exploration. The work attempts to improve anti-pigmentation therapy by encapsulating AZA in mesoporous silica nanoparticles (MSNs) in a gel matrix. While the data show that AZA-MSNs have notable entrapment efficiency and increased drug loading capacities, the study is mostly based on structural elucidation, *in-vitro* and *ex-vivo* rat skin permeation tests, which limits direct extrapolation to human skin in vivo. Appropriately sized amorphous particles with a porous structure, increased surface area, improved penetration, amorphous drug incorporation, and strong thermal stability showed that this method delivers azelaic acid deeper into the skin appropriately. The long-term stability and biocompatibility of the formulation remain unknown, underscoring the need for additional research, including extended stability testing. Clinical validation through human trials is critical for proving the formulation's efficacy, safety, and tolerance in real-world applications. Future goals include optimizing the formulation, scaling up production methods, and investigating combination medicines for better treatment outcomes. Addressing these limitations and following proposed future possibilities will be beneficial in realizing AZA's full therapeutic potential of MSN-gel for pigmentation therapy.

Funding

The author(s) declare that financial support was received by the Researchers Supporting Project (RSP2024R301), King Saud University, Riyadh, Saudi Arabia.

Data availability statement

The data will be made available upon reasonable request.

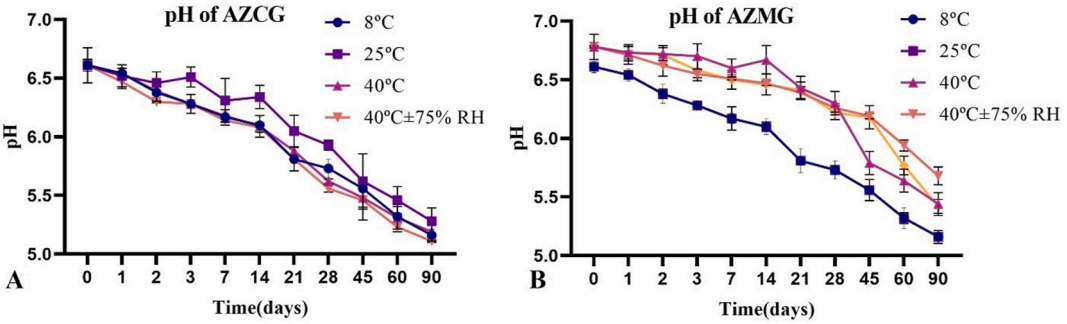

Fig. 8. pH of AZCG (A) and AZMG (B) after storage under different conditions.

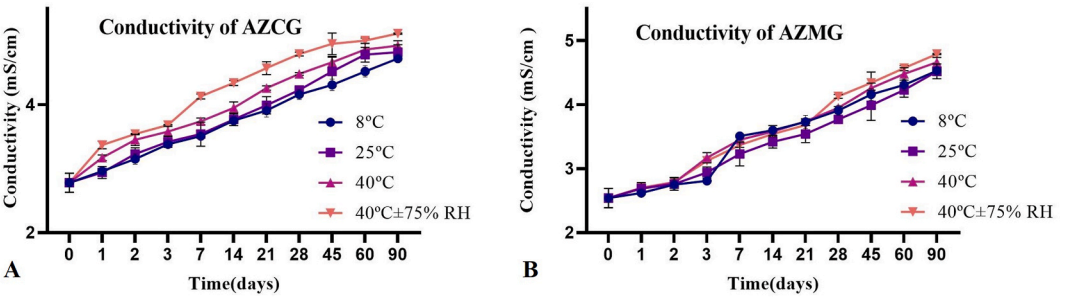

Fig. 9. Conductivity of AZCG (A) and AZMG (B) after storage under different conditions.

CRediT authorship contribution statement

Tahreem Arshad: Writing – review & editing, Writing – original draft, Project administration, Methodology, Investigation, Data curation. **Haji Muhammad Shoaib Khan:** Visualization, Supervision, Software, Conceptualization. **Naveed Akhtar:** Visualization, Validation. **Hanasul Hanan:** Writing – review & editing. **Muhammad Delwar Hussain:** Validation, Software. **Mohsin Kazi:** Writing – review & editing, Visualization, Funding acquisition.

Declaration of competing interest

The authors declare that they have no known competing financial interests or personal relationships that could have appeared to influence the work reported in this paper.

Acknowledgments

The authors would like to extend their sincere appreciation to the Researchers Supporting Project Number (RSP2024R301), King Saud University, Riyadh, Saudi Arabia.

References

[1] E. N, et al., Human Anatomy & Physiology, eleventh ed., Pearson Education, 2011.
[2] Y. Gilaberte, et al., Anatomy and function of the skin, Nanoscience in Dermatology (2016) 1–14.
[3] S.R. Desai, Hyperpigmentation therapy: a review, The Journal of clinical and aesthetic dermatology 7 (8) (2014) 13.
[4] A. Nautiyal, S. Wairkar, Management of hyperpigmentation: current treatments and emerging therapies, Pigment cell & melanoma research 34 (6) (2021) 1000–1014.
[5] Y. Yamaguchi, V.J. Hearing, Physiological factors that regulate skin pigmentation, Biofactors 35 (2) (2009) 193–199.
[6] M.S. Ke, T. Soriano, G.P. Lask, Optimal treatments for hyperpigmentation, J. Cosmet. Laser Ther. 8 (1) (2006) 7–13.
[7] S. Jafari, et al., Mesoporous silica nanoparticles for therapeutic/diagnostic applications, Biomed. Pharmacother. 109 (2019) 1100–1111.
[8] I. Slowing, B.G. Trewyn, V.S.-Y. Lin, Effect of surface functionalization of MCM-41-type mesoporous silica nanoparticles on the endocytosis by human cancer cells, J. Am. Chem. Soc. 128 (46) (2006) 14792–14793.
[9] A.C. Breathnach, et al., Azelaic acid therapy in disorders of pigmentation, Clin. Dermatol. 7 (2) (1989) 106–119.
[10] L.M. Baliña, K. Graupe, The treatment of melasma 20% azelaic acid versus 4% hydroquinone cream, Int. J. Dermatol. 30 (12) (1991) 893–895.
[11] J. Gibson, Rationale for the development of new topical treatments for acne vulgaris, Cutis 57 (1 Suppl) (1996) 13–19.
[12] M. Nazzaro-Porro, Azelaic acid, J. Am. Acad. Dermatol. 17 (6) (1987) 1033–1041.
[13] A. Breathnach, M. Nazzaro-Porro, S. Passi, Azelaic acid, Br. J. Dermatol. 111 (1) (1984) 115–120.
[14] K. Graupe, et al., Efficacy and safety of topical azelaic acid (20 percent cream): an overview of results from European clinical trials and experimental reports, Cutis 57 (1 Suppl) (1996) 20–35.

[15] Q.H. Nguyen, T.P. Bui, Azelaic acid: pharmacokinetic and pharmacodynamic properties and its therapeutic role in hyperpigmentary disorders and acne, Int. J. Dermatol. 34 (2) (1995) 75–84.
[16] A. Breathnach, Pharmacological properties of azelaic acid: a rationale for clinical use, Clin. Drug Invest. 10 (1995) 27–33.
[17] D. Bergman, J. Luke, Azelaic acid, Journal of the Dermatology Nurses' Association 9 (3) (2017) 157–160.
[18] A. Budiman, D.L. Aulifa, Encapsulation of drug into mesoporous silica by solvent evaporation: a comparative study of drug characterization in mesoporous silica with various molecular weights, Heliyon 7 (12) (2021) 12345.
[19] C. Xu, C. Lei, C. Yu, Mesoporous silica nanoparticles for protein protection and delivery, Front. Chem. 7 (2019) 290.
[20] Y. Huang, et al., Silica nanoparticles: biomedical applications and toxicity, Biomed. Pharmacother. 151 (2022) 113053.
[21] M. Rani, et al., Formulation development and characterization of luliconazole loaded− mesoporous silica nanoparticles (MCM− 48) as topical hydrogel for the treatment of cutaneous candidiasis, J. Drug Deliv. Sci. Technol. 91 (2024) 105250.
[22] G.F. Andrade, et al., Surface modification and biological evaluation of kojic acid/silica nanoparticles as platforms for biomedical systems, Int. J. Appl. Ceram. Technol. 17 (1) (2020) 380–391.
[23] A. Lodha, et al., Synthesis of mesoporous silica nanoparticles and drug loading of poorly water soluble drug cyclosporin A, J. Pharm. BioAllied Sci. 4 (Suppl 1) (2012) S92.
[24] S.N. Harun, et al., Synthesis and optimization of mesoporous silica nanoparticles for ruthenium polypyridyl drug delivery, Pharmaceutics 13 (2) (2021) 150.
[25] A.A. Kajani, et al., Carbon dot incorporated mesoporous silica nanoparticles for targeted cancer therapy and fluorescence imaging, RSC Adv. 13 (14) (2023) 9491–9500.
[26] M.R. Amin, M.A. Chowdhury, M.A. Kowser, Characterization and performance analysis of composite bioplastics synthesized using titanium dioxide nanoparticles with corn starch, Heliyon 5 (8) (2019) 12345.
[27] F.G.L. Medeiros Borsagli, I.C. Carvalho, H.S. Mansur, Amino acid-grafted and N-acylated chitosan thiomers: construction of 3D bio-scaffolds for potential cartilage repair applications, Int. J. Biol. Macromol. 114 (2018) 270–282.
[28] H. Hanan, et al., Revolutionizing colon cancer therapy by site-specific 5-fluorouracil delivery with novel stimuli-responsive mucoadhesive hydrogel: optimization via response surface methodology, J. Drug Deliv. Sci. Technol. (2024) 105358.
[29] Y.M. Kim, et al., Oxyresveratrol and hydroxystilbene compounds inhibitory effect on tyrosinase and mechanism of action, J. Biol. Chem. 277 (18) (2002) 16340–16344.
[30] H.M.S. Khan, et al., Encapsulation of alpha arbutin, a depigmenting agent, in nanosized ethosomes: invitro and invivo human studies, Heliyon 9 (9) (2023) 12345.
[31] T. Arshad, et al., Invitro and split-faced placebo-controlled invivo study on the skin rejuvenating effects of cream loaded with bioactive extract of Indigofera argentea burm. f, Front. Pharmacol. 15 (2023) 1352045.
[32] W. Liang, et al., Organic matters adsorbed on goethite inhibited the heterogeneous aggregation and adsorption of CdSe quantum dots: experiments and extended DLVO theory, J. Hazard Mater. (2024) 133769.
[33] R.H. Müller, K. Mäder, S. Gohla, Solid lipid nanoparticles (SLN) for controlled drug delivery–a review of the state of the art, Eur. J. Pharm. Biopharm. 50 (1) (2000) 161–177.
[34] F.N. Sorasitthiyanukarn, et al., Stability and biological activity enhancement of fucoxanthin through encapsulation in alginate/chitosan nanoparticles, Int. J. Biol. Macromol. (2024) 130264.
[35] V. Ambrogi, et al., Improvement of dissolution rate of piroxicam by inclusion into MCM-41 mesoporous silicate, Eur. J. Pharmaceut. Sci. 32 (3) (2007) 216–222.
[36] F. Qu, et al., Bio-templated synthesis of highly ordered macro-mesoporous silica material for sustained drug delivery, Solid State Sci. 12 (2010) 851–856.
[37] M.K. Iqubal, et al., Topical delivery of Mannose Conjugated-Doxorubicin-Berberine nanostructured lipid carrier gel for skin cancer amelioration: formulation optimization, in-silico, in-vitro, ex-vivo assessment, and dermatokinetic analysis, J. Drug Deliv. Sci. Technol. 93 (2024) 105378.
[38] K.S. Sing, Reporting physisorption data for gas/solid systems with special reference to the determination of surface area and porosity (Provisional), Pure Appl. Chem. 54 (11) (1982) 2201–2218.
[39] M. Manzano, et al., Studies on MCM-41 mesoporous silica for drug delivery: effect of particle morphology and amine functionalization, Chem. Eng. J. 137 (1) (2008) 30–37.
[40] V. Cauda, A. Schlossbauer, T. Bein, Bio-degradation study of colloidal mesoporous silica nanoparticles: effect of surface functionalization with organo-silanes and poly (ethylene glycol), Microporous Mesoporous Mater. 132 (1–2) (2010) 60–71.
[41] Y. Zhang, et al., Spherical mesoporous silica nanoparticles for loading and release of the poorly water-soluble drug telmisartan, J. Contr. Release 145 (3) (2010) 257–263.
[42] F. Furlani, et al., Designing bioinspired multifunctional nanoplatforms to support wound healing and skin regeneration: Mg-hydroxyapatite meets melanins, Colloids Surf. B Biointerfaces 235 (2024) 113756.
[43] W.M. Abdelwahab, et al., Co-delivery of a novel lipidated TLR7/8 agonist and hemagglutinin-based influenza antigen using silica nanoparticles promotes enhanced immune responses, Pharmaceutics 16 (1) (2024) 107.
[44] K. Khezri, V. Haddadi-Asl, H. Roghani-Mamaqani, Introduction of a double bond containing modifier on the surface of MCM-41 nanoparticles: application for SR&NI ATRP of styrene, Nano 9 (2) (2014) 1450023.
[45] H. Hanan, et al., Revolutionizing colon cancer therapy by site-specific 5-fluorouracil delivery with novel stimuli-responsive mucoadhesive hydrogel: optimization via response surface methodology, J. Drug Deliv. Sci. Technol. 92 (2024) 105358.
[46] R. Das, M.D. Adhikari, P.S. Chauhan, Future directions in nanomaterials research for biological applications, Nanoparticle Toxicity and Compatibility 161 (2024) 1–26.
[47] J. Manosroi, et al., Enhancement of the release of azelaic acid through the synthetic membranes by inclusion complex formation with hydroxypropyl-β-cyclodextrin, Int. J. Pharm. 293 (1–2) (2005) 235–240.
[48] G. Quan, et al., Lactosaminated mesoporous silica nanoparticles for asialoglycoprotein receptor targeted anticancer drug delivery, J. Nanobiotechnol. 13 (1) (2015) 1–12.
[49] P.-W. Hsieh, et al., The co-drug of conjugated hydroquinone and azelaic acid to enhance topical skin targeting and decrease penetration through the skin, Eur. J. Pharm. Biopharm. 81 (2) (2012) 369–378.
[50] U. Ciesla, F. Schüth, Ordered mesoporous materials, Microporous Mesoporous Mater. 27 (2–3) (1999) 131–149.
[51] S. Kapoor, R. Hegde, A.J. Bhattacharyya, Influence of surface chemistry of mesoporous alumina with wide pore distribution on controlled drug release, J. Contr. Release 140 (1) (2009) 34–39.
[52] Y. Hu, et al., 3D cubic mesoporous silica microsphere as a carrier for poorly soluble drug carvedilol, Microporous Mesoporous Mater. 147 (2012) 94–101.
[53] S. Chawla, et al., Mechanism of tyrosinase inhibition by deoxyarbutin and its second-generation derivatives, Br. J. Dermatol. 159 (6) (2008) 1267–1274.
[54] V.K. Sharma, et al., In vitro anti-tyrosinase activity of 5-(hydroxymethyl)-2-furfural isolated from Dictyophora indusiata, Phytother Res.: An International Journal Devoted to Pharmacological and Toxicological Evaluation of Natural Product Derivatives 18 (10) (2004) 841–844.
[55] E. Ugazio, et al., Thermoresponsive mesoporous silica nanoparticles as a carrier for skin delivery of quercetin, Int. J. Pharm. 511 (1) (2016) 446–454.
[56] S. Sapino, et al., Mesoporous silica nanoparticles as a promising skin delivery system for methotrexate, Int. J. Pharm. 530 (1–2) (2017) 239–248.
[57] M.T. Gregolin, et al., Rheological characterization of hydrophylic gels, J. Dispersion Sci. Technol. 31 (6) (2010) 820–825.
[58] W. Arshad, et al., Polymeric emulgel carrying Cinnamomum tamala extract: promising delivery system for potential topical applications, Brazilian Journal of Pharmaceutical Sciences 56 (2020).
[59] P.N. Dave, P.M. Macwan, B. Kamaliya, The effect of adding cobalt ferrite (CoFe3O4) nanoparticles as fillers on rheological and structural behaviour of gum ghatti-cl-poly (NIPAm) hydrogels, Mech. Time-Dependent Mater. (2024) 1–30.
[60] B. da Silva Gomes, et al., Beyond the adverse effects of the systemic route: exploiting nanocarriers for the topical treatment of skin cancers, Adv. Drug Deliv. Rev. (2024) 115197.

[61] P. Khan, N. Akhtar, Phytochemical investigations and development of ethosomal gel with Brassica oleraceae L.(Brassicaceae) extract: an innovative nano approach towards cosmetic and pharmaceutical industry, Ind. Crop. Prod. 183 (2022) 114905.
[62] L. Fetouhi, J. Martinez-Vega, B. Petitgas, Electric conductivity, aging and chemical degradation of polyesterimide resins used in the impregnation of rotating machines, IEEE Trans. Dielectr. Electr. Insul. 25 (1) (2018) 294–305.
[63] M. Agarwal, Y.M. Joshi, Signatures of physical aging and thixotropy in aqueous dispersion of Carbopol, Phys. Fluids 31 (6) (2019).
[64] K. Sghier, et al., Novel therapeutic hybrid systems using hydrogels and nanotechnology: a focus on nanoemulgels for the treatment of skin diseases, Gels 10 (1) (2024) 45.